# Supplementary Information

# Continuous Electrical Pumping Membrane Process for Seawater Lithium Mining

Zhen Li, Chunyang Li, Xiaowei Liu, Li Cao, Peipei Li, Ruicong Wei, Xiang Li, Dong Guo, Kuo-Wei Huang, Zhiping Lai*

Division of Physicals Science and Engineering, King Abdullah University of Science and Technology (KAUST), Thuwal, 23955-6900, Saudi Arabia

*Corresponding Author: Zhiping Lai (Zhiping.lai@kaust.edu.sa)

## (1) Supplementary tables

| Process | Li concentration of feed solution (ppm) | Li/Mg selectivity | Li/Na Selectivity | Voltage (V) | Lithium extraction rate mg/(ppm·dm$^2$·h) | Literature |
|---|---|---|---|---|---|---|
| Nanofiltration membranes | 700 | 11.33 | - | 1.75 | 0.21 | [1] |
| Bipolar membrane | 159 | 30 | - | 15 | 4.30 | [2] |
| Liquid-membrane | 1000 | 15 | - | 3.00 | 12.96 | [3] |
| Ionic liquid membrane | 0.17 | 39.7 | 0.80 | 3.00 | 7.59 | [4] |
| Si doped LATP | 0.17 | - | - | 0.04 | 0.97 | [5] |
| LATP | 0.17 | - | - | 4.52 | 11.18 | [6] |
| **Glass-type LLTO** | **0.21** | **4.5 million[a]** | **1.7 million[a]** | **3.25** | **13.43[b]** | **This study** |

a. The selectivity of our process is the nominal selectivity that is calculated based on the data after 5 stages.
b. The lithium extraction rate is calculated from the first stage.

Table S1. Comparison of the lithium extraction rate in literatu

## (2) Supplementary Figures

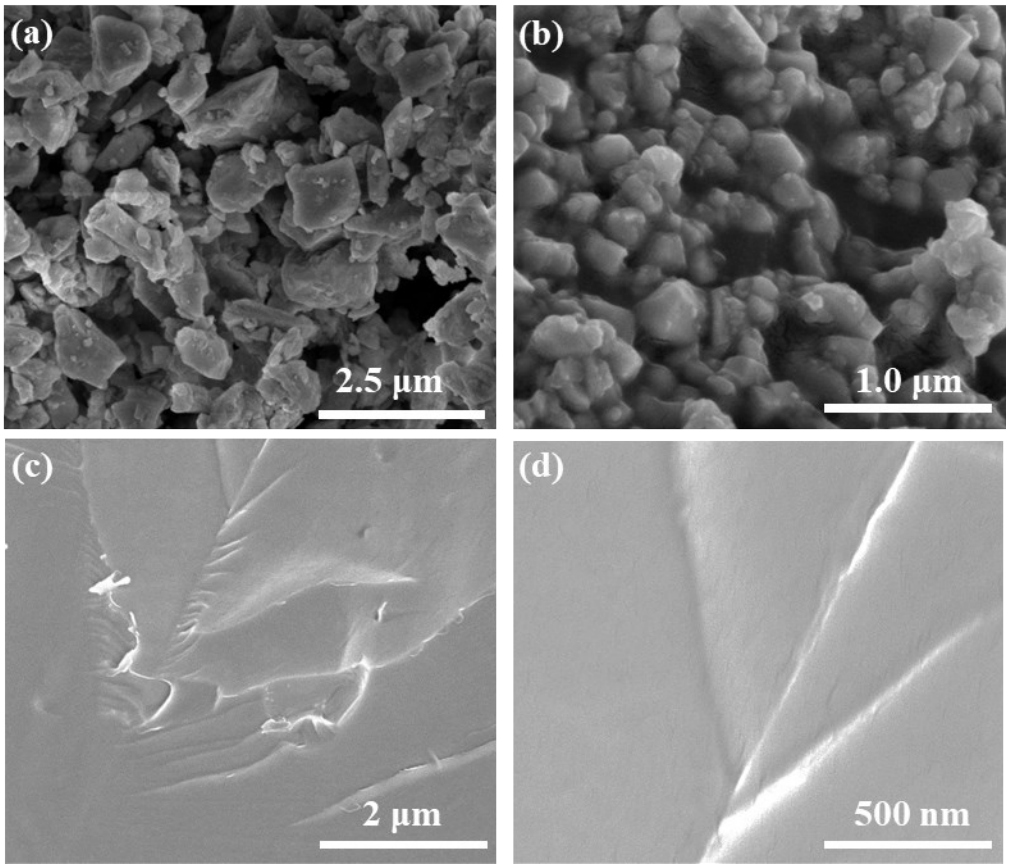


**Figure S1**: (a) SEM images of the LLTO particles prepared via the sol-gel method; (b) SEM images of the LLTO nanoparticles after ball-milling. (c) and (d) High magnification SEM image of the LLTO membrane.

Figure S1 reveals that the as-prepared LLTO particles ranged in size from 1.0–2.0 µm, and that they were irregularly shaped. After ball milling, LLTO nanoparticles were formed with an average diameter of 200 nm. The LLTO membrane has a dense and smooth surface with no grainboundaries.

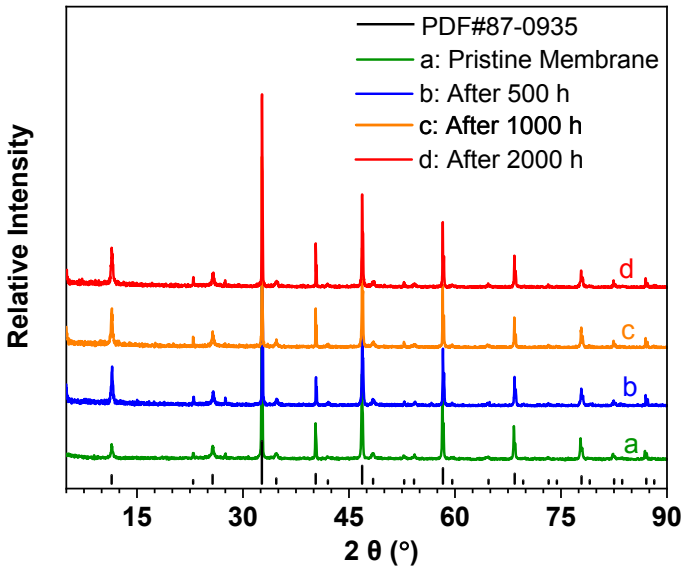


**Figure S2**. XRD patterns of the LLTO membranes after different durations of usage.

Figure S2 shows that the LLTO membrane consists of high-purity $Li_{0.33}La_{0.57}TiO_3$ without any impurities being present. The XRD pattern of the LLTO membrane was well preserved after 2000 h of usage, indicating its good stability and durability.

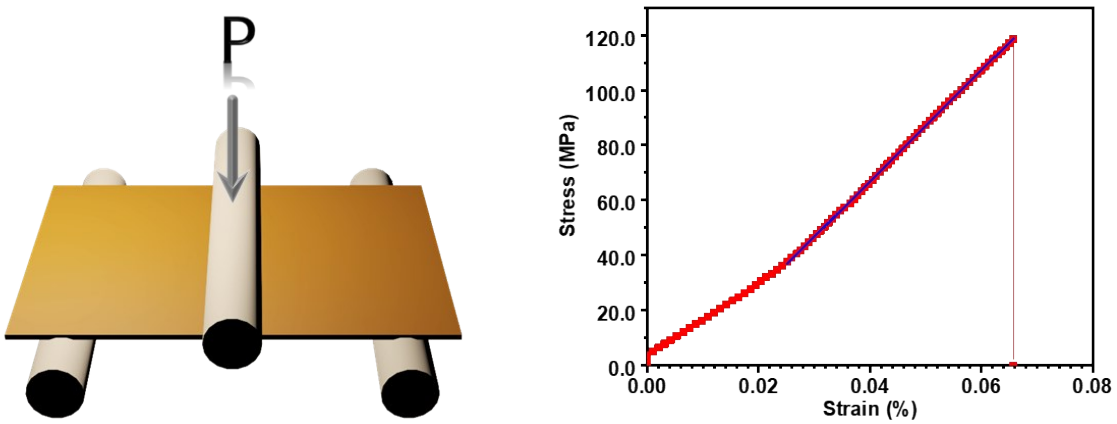


**Figure S3**. Mechanical property of the LLTO membrane tested by three-point flexural test.

The LLTO sample for mechanical property testing was polished into a rectangle with size of 8.0×5.67 mm$^2$ ($L$'×$W$), and then placed on two supporting cylinders. The space ($L$, mm) between the two supporting cylinders is 6.03 mm. Another cylinder was placed on top of the LLTO sample at the middle point, and applied load with a increasing rate of 0.06 N min$^{-1}$. The deflection ($f$, mm) and loading ($P$, N) was recorded using a dynamic mechanical analyzer (TA Instruments DMA Q800) at 25 °C. The thickness ($h$, mm) of the LLTO sample was 0.065 mm. The stress ($\sigma_f$) and strain ($\varepsilon_f$) were calculated to be 118.51 MPa and 0.066% by Equation S1 and S2, respectively. The modulus ($E$) was calculated to be 201.5 GPa from the slope in Figure S3.

$$\sigma_f = \frac{1}{4}PL \Big/ \left(\frac{1}{6}Wh^2\right) \qquad \text{Equation S1}$$

$$\varepsilon_f = 6fW/L^2 \qquad \text{Equation S2}$$

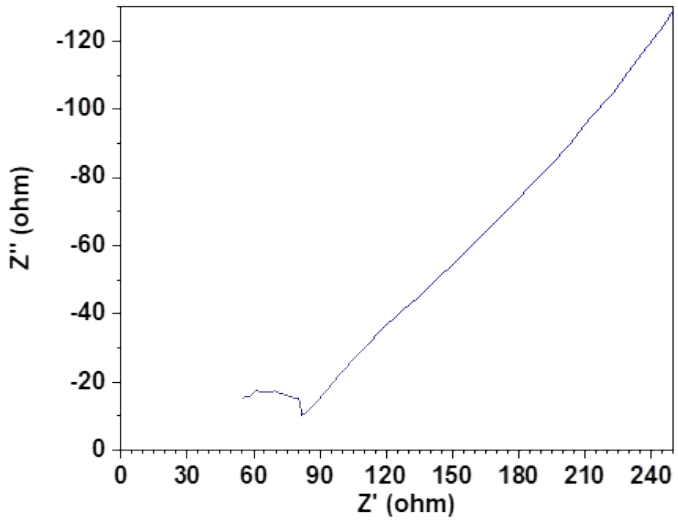


**Figure S4**. Electrochemical impedance spectroscopy of the LLTO membrane.

The electrochemical impedance spectrum of the LLTO membrane was acquired using a CHI© electrochemical workstation between 1.0 MHz and 1 Hz. The sample was initially sprayed with Ir to give a 15 nm-thick coating, then sandwiched by two carbon cloths to improve the contact between the membrane and the electrode. The obtained result reveals the impedance of LLTO membrane was ~82 ohms, indicating its high lithium permeability.

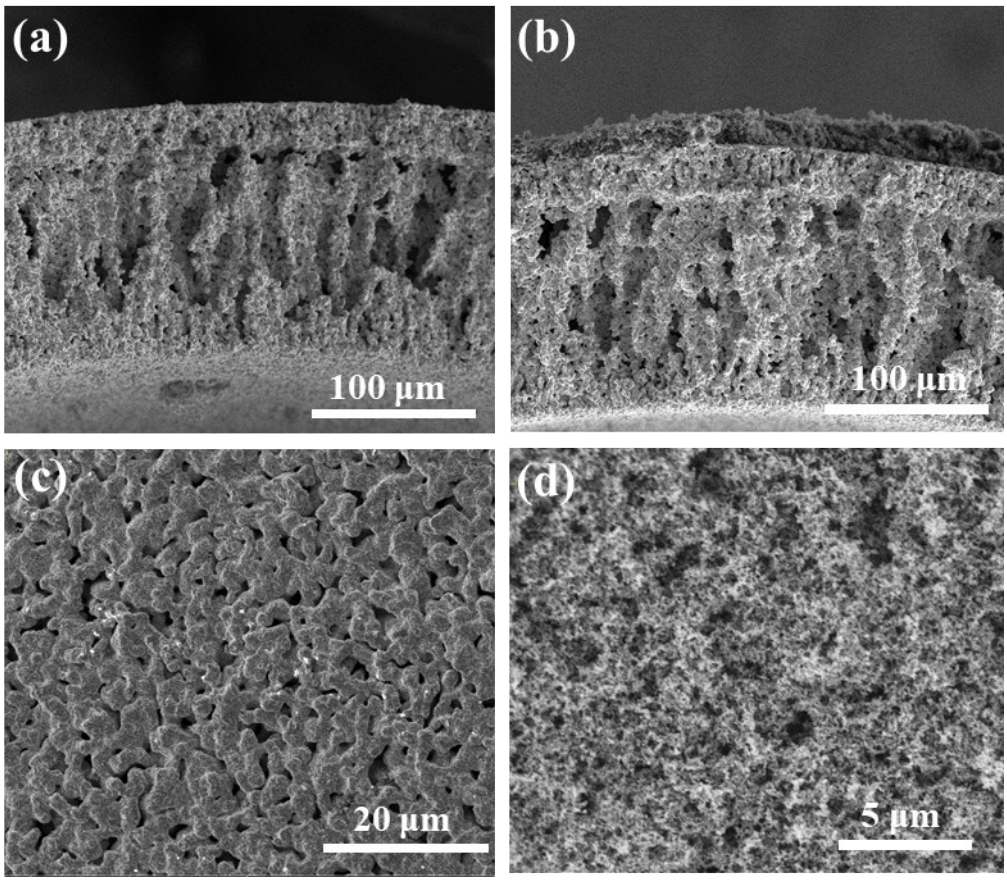


**Figure S5.** (a) SEM image of the cross-section of the raw copper hollow fibre; (b) SEM image of the cross-section of the catalytic Pt/Ru coated copper hollow fibre; (c) SEM image of the outside surface of the raw copper hollow fibre; and (d) SEM image of the outside surface of catalytic Pt/Ru coated copper hollow fibre.

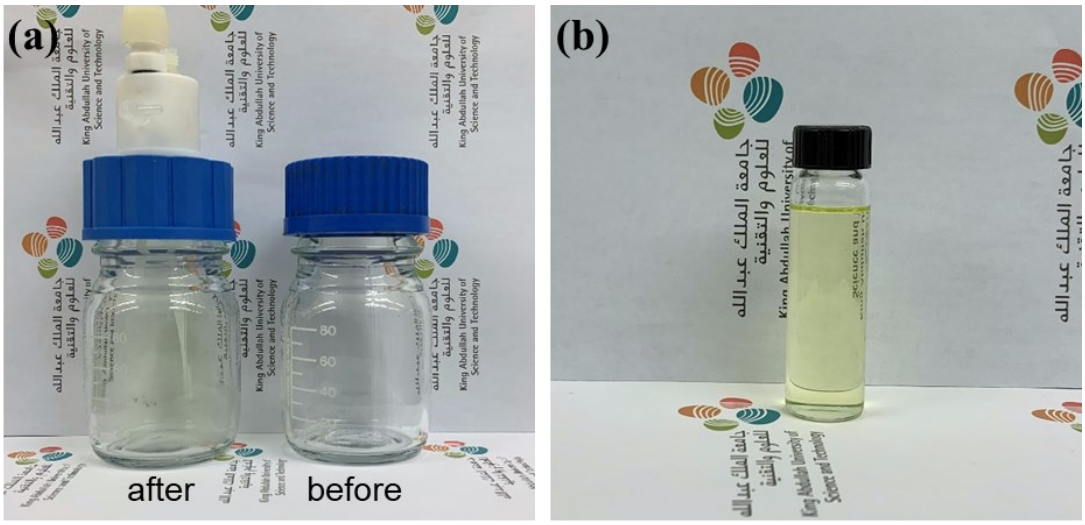


**Figure S6**. (a) Photographic images of the bottle before and after collection of the released $Cl_2$ during the lithium enrichment process. (b) Photographic image of the $CCl_2H_2$ solution after absorption of the released $Cl_2$.

Figure S6 shows the $Cl_2$ gas collected from the anode compartment of the lithium enrichment system. After dissolving in $CCl_2H_2$, the typical yellow-green appearance of $Cl_2$ can be observed.

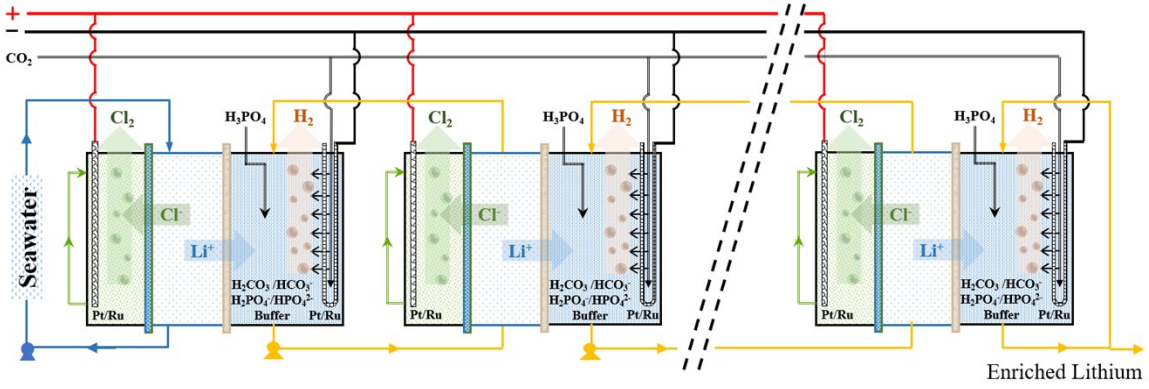


**Figure S7**. Conceptual design of continuous multi-step membrane process for lithium extraction.

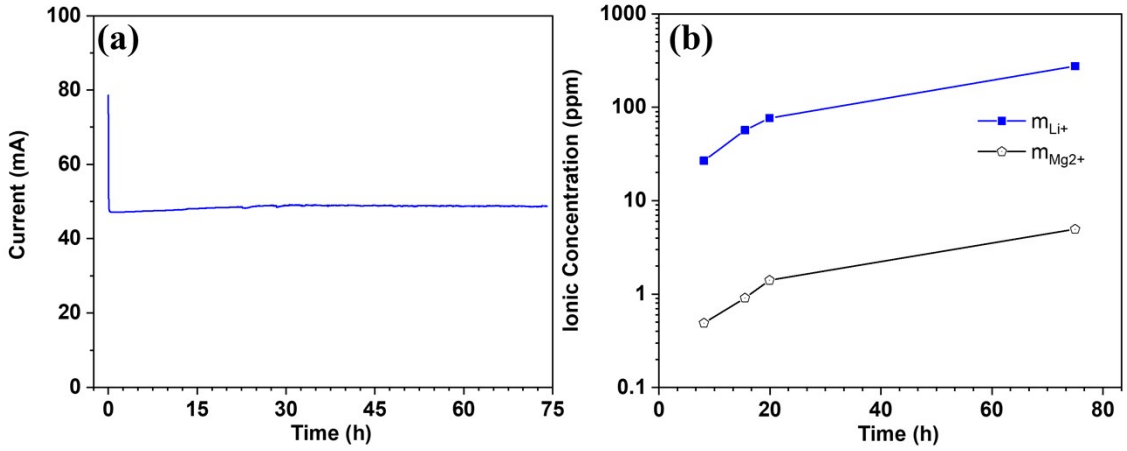


**Figure S8**. Extended lithium extraction from seawater by a single-step process (membrane area = 2.01 $cm^2$). (a) Chronoamperometric curve of a single-step lithium extraction from seawater for up to 75 hours. (b) $Li^+$ and $Mg^{2+}$ concentrations vs. time in the enriched solution.

The stable chronoamperometry curves shown in Figure S8a demonstrate that the lithium enrichment system can function at a current of 49±3 μA, and that it exhibits long-term stability under these conditions. The $Li^+$ and $Mg^{2+}$ concentrations were tested at 7.5, 15, 21, and 75 h using ICP-OES, as outlined in Figure S8b. The $Li^+$ and $Mg^{2+}$ concentrations increased over time by a ratio of ~56. According to the requirements of lithium battery-grade purity (China standard, YS/T582-2013), the $Mg^{2+}$ content in the final salt product should be <70 ppm, implying that the $Li^+/Mg^{2+}$ ratio in the enriched lithium solution should be >2609. This result indicates that a multi-step process is necessary to achieve a high-purity product.

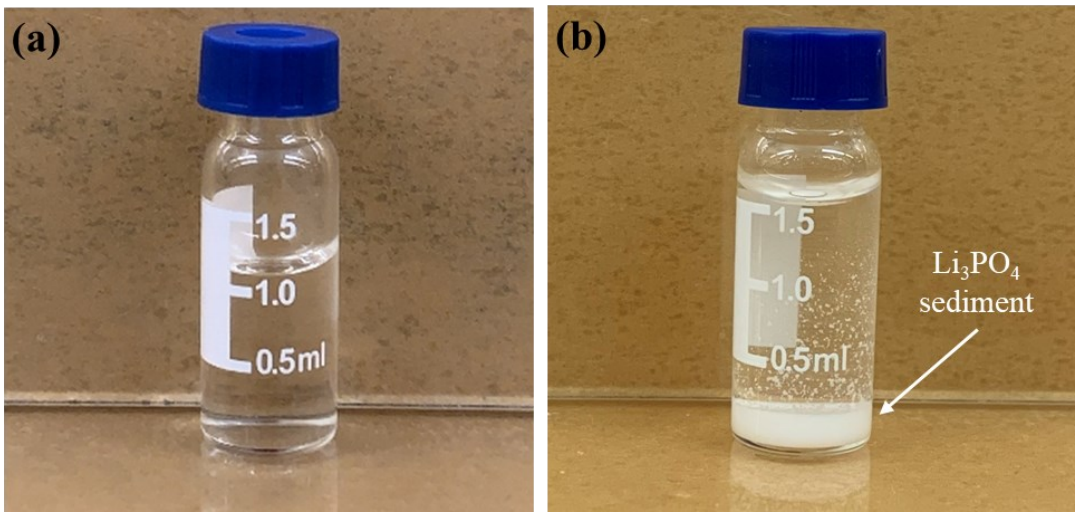


**Figure S9.** (a) The enriched lithium solution after 5 stages. (b) The $Li_3PO_4$ product precipitated from the enriched lithium solution after 5 stages.

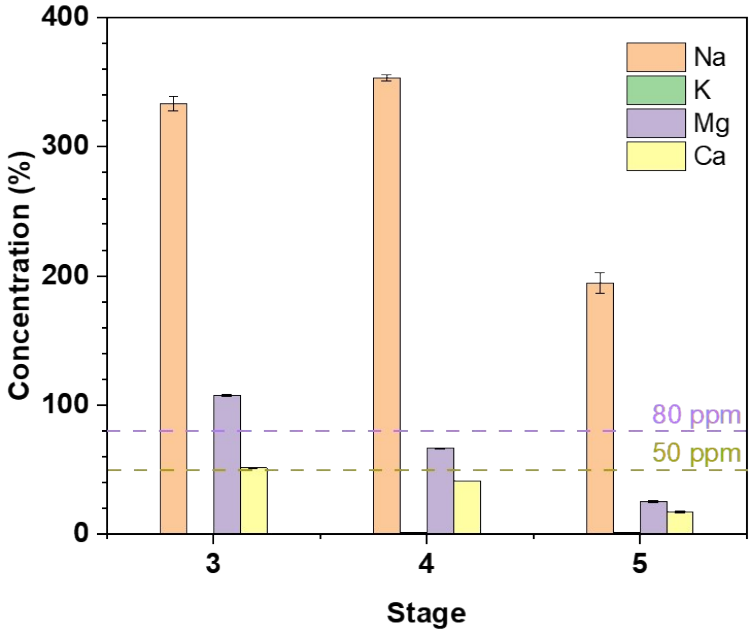


**Figure S10.** The contents of products precipitated after the 3rd, 4th and 5th stages.

## Reference:


1. Sheng, F., Hou, L., Wang, X., Irfan, M., Shehzad, M.A., Wu, B., Ren, X., Ge, L., and Xu, T. *J. Membr. Sci.* 2020 **594**, 117453.
2. Qiu, Y., Yao, L., Tang, C., Zhao, Y., Zhu, J., and Shen, J. *Desalination* 2019 **465**, 1-12.
3. Zhao, Z., Liu, G., Jia, H., and He, L. *J. Membr. Sci.* 2020 **596**, 117685.
4. Hoshino, T. *Fusion Eng. Des.* 2013 **88**, 2956-2959.
5. Hoshino, T. *Desalination* 2015 **359**, 59-63.
6. Yang, S., Zhang, F., Ding, H., He, P., and Zhou, H. 2018 ***Joule*** 2, 1648-1651.